Nonlinear self-channeling and beam shaping of magnetostatic waves in ferromagnetic films

J. W. Boyle, S. A. Nikitov,* A. D. Boardman, J. G. Booth, and K. Booth
Photonics and Nonlinear Science Group, Joule Laboratory, Department of Physics, University of Salford, Salford, M5 4WT, United Kingdom

(Received 13 December 1994; revised manuscript received 3 November 1995)

Self-channeling and nonlinear beam shaping of magnetostatic waves in thin in-plane magnetized yttrium-iron-garnet films have been observed. Different power levels of a cw signal were launched into a magnetic film using a short microstrip antenna. A Brillouin light scattering system was used to observe the profile of the beams. Self-channeling of the magnetostatic wave beam occurred because of the interplay between the diffraction of the beam and nonlinearity, which leads to self-focusing. This was observed as the input power reached a threshold value equal to a few hundred milliwatts. A discussion of the observations is presented, together with estimates of the parameter ranges. [S0163-1829(96)01418-X]

I. INTRODUCTION

Yttrium-iron-garnet (YIG) films, in an external magnetic field, are very good test beds for investigating the nonlinear properties of magnetostatic waves. For example, the last decade has produced a series of experiments directed toward the observation of bright[1–5] and dark[6] envelope solitons. In the linear domain there has been a number of experimental measurements[7–10] of the spatial characteristics of magnetostatic waves that have used induction and light probing methods. There have even been measurements of nonlinear magnetostatic wave beam propagation at high power levels, in films magnetized perpendicular to the film plane,[11] and in films magnetized in plane when three-magnon decay processes are allowed.[12]

In this paper we report experimental observation of the nonlinear beam evolution of magnetostatic waves propagating in a ferromagnetic film magnetized in plane, at frequencies where three-magnon decay is suppressed.[12] The possibility of magnetostatic wave self-channeling was predicted in the classic paper by Zvezdin and Popkov,[13] in which the theory of magnetostatic wave solitons was established. Explained briefly, nonlinear beam shaping, which may lead to self-channeling, occurs when the natural tendency of the magnetostatic wave beam to diffract is modified by the power level. For example, when diffraction is opposed by nonlinearity, *spatial solitons* may form, in principle. Since a YIG film must have an applied magnetic field in order to align the spins, it supports an anisotropic system of magnetostatic spin waves, which fall into three types. Two of these arise when the external magnetic field is applied parallel to the plane of the film. Respectively, these are *surface waves*, propagating perpendicularly to the magnetic field, and *backward volume waves*. The details of the dispersion curves associated with these waves are readily available in the literature[13] and need not be discussed here. Of all the possible types of magnetostatic waves that can occur in a YIG film, only magnetostatic backward volume waves can exhibit self-channeling[13] and evolve into spatial solitons.

Nonlinearity can cause the spin wave beam to focus or defocus depending upon the type of wave. Since such focusing, or defocusing, is caused by the power of the wave itself, it is usually called *self-focusing*, i.e., channeling, or *self-defocusing*. Even in real YIG films, in which magnetic losses can influence strongly the conditions for the appearance of any form of self-channeling, such an effect should occur. This paper provides experimental evidence of it.

II. THEORETICAL BACKGROUND

Of the three principal magnetostatic wave types (two of which are found in a ferromagnetic film magnetized in plane), the work of Zvezdin and Popkov[13] shows that only backward volume wave modes have the necessary transverse properties to lead to self-focusing. Unfortunately, the backward volume wave configuration can also lead to longitudinal modulational instability, which can cause any spatial soliton formed to become unstable. It is necessary, therefore, to decide whether these two effects, transverse instability, resulting in spatial solitons, and longitudinal instability, can be observed separately or whether experiment forces both effects to be observed simultaneously. Recent work by Chen *et al.*[4] shows that if pulses of backward volume waves are used, then longitudinal effects dominate over self-focusing effects. It would be convenient if, by using beams, self-focusing (transverse) effects dominate over dispersion (longitudinal) effects, but it is not self-evident, for backward volume waves, what will occur. In order to proceed it is useful to add to the work of Zvezdin and Popkov a formal discussion of the propagation of a magnetostatic wave beam. First, although the beam as a whole may be propagating in a direction perpendicular, or parallel, to an applied magnetic field, the partial plane waves, making up the beam, travel at various angles to this direction. For a beam traveling principally *along the y direction*, in the (yz) plane, the magnetostatic potential associated with the *bundle* of waves is

$$\phi(x,y,z,t)=\frac{1}{2}\left[\int_0^\infty\int_{-\infty}^{\infty}C(k_\parallel,k_\perp)f(k_\parallel,k_\perp,x)e^{i[k_\parallel y+k_\perp z-\omega(k_\parallel,k_\perp)t]}dk_\perp dk_\parallel+\text{c.c.}\right], \tag{1}$$

where $f(k_\parallel,k_\perp,x)$ is the modal profile. The guided mode is assumed to be confined in the x direction, and it will be assumed here that the Fourier amplitude defined by $C(k_\parallel,k_\perp)$ is sufficiently well localized around the propagation direction $[k=k_\parallel, k_\perp\approx 0]$ for $f(k_\parallel,k_\perp,x)$ to be only weakly dependent upon $k_\parallel$ and $k_\perp$. By defining the *small* deviations $k_\parallel'=k_\parallel-k$ and $\Delta\omega=\omega(k+k_\parallel',k_\perp)-\omega(k,0)$, $\phi(x,y,z,t)$ may be approximated to

$$\phi(x,y,z,t)=\tfrac{1}{2}[f(k,0,x)A(y,z,t)e^{i[ky-\omega(k,0)t]}+\text{c.c.}], \tag{2}$$

where

$$\frac{\partial A}{\partial t}(y,z,t)=\int_{-k}^{\infty}\int_{-\infty}^{\infty}C(k+k_\parallel',k_\perp)e^{i(k_\parallel' y+k_\perp z-\Delta\omega t)}[-i\Delta\omega]dk_\perp dk_\parallel' \tag{3}$$

and

$$\Delta\omega=\Delta\omega(0,0)+\left(\frac{\partial\Delta\omega(k_\parallel',0)}{\partial k_\parallel'}\right)_{k_\parallel'=0}k_\parallel'+\left(\frac{\partial\Delta\omega(0,k_\perp)}{\partial k_\perp}\right)_{k_\perp=0}k_\perp+\left(\frac{\partial^2\Delta\omega(k_\parallel',k_\perp)}{\partial k_\parallel'\partial k_\perp}\right)_{k_\parallel'=0,k_\perp=0}k_\parallel'k_\perp$$
$$+\frac{1}{2}\left(\frac{\partial^2\Delta\omega(k_\parallel',0)}{\partial k_\parallel'^2}\right)_{k_\parallel'=0}k_\parallel'^2+\frac{1}{2}\left(\frac{\partial^2\Delta\omega(0,k_\perp)}{\partial k_\perp^2}\right)_{k_\perp=0}k_\perp^2+\cdots. \tag{4}$$

Now $\Delta\omega(0,0)=0$ and $\Delta\omega(k_\parallel',k_\perp)$ is an odd function of $k_\perp$; so

$$\left(\frac{\partial\Delta\omega(0,k_\perp)}{\partial k_\perp}\right)_{k_\perp=0}=0$$

and

$$\left(\frac{\partial^2\Delta\omega(k_\parallel',k_\perp)}{\partial k_\parallel\partial k_\perp}\right)_{k_\parallel'=0,k_\perp=0}=0.$$

Therefore,

$$\Delta\omega=\left(\frac{\partial\Delta\omega(k_\parallel',0)}{\partial k_\parallel'}\right)_{k_\parallel'=0}k_\parallel'+\frac{1}{2}\left(\frac{\partial^2\Delta\omega(k_\parallel',0)}{\partial k_\parallel'^2}\right)_{k_\parallel'=0}k_\parallel'^2+\frac{1}{2}\left(\frac{\partial^2\Delta\omega(0,k_\perp)}{\partial k_\perp^2}\right)_{k_\perp=0}k_\perp^2+\cdots. \tag{5}$$

Hence, up to orders of $k_\parallel'^2$ and $k_\perp^2$, and because $\Delta\omega(k_\parallel',0)=\omega(k+k_\parallel',0)-\omega(k,0)$, the *linear* envelope equation is

$$i\left[\frac{\partial A(y,z,t)}{\partial t}+\left(\frac{\partial\omega(k,0)}{\partial k}\right)\frac{\partial A(y,z,t)}{\partial y}\right]+\frac{1}{2}\left(\frac{\partial^2\omega(k,0)}{\partial k^2}\right)\frac{\partial^2A(y,z,t)}{\partial y^2}y+\frac{1}{2}\left[\frac{\partial^2\omega(k,k_\perp)}{\partial k_\perp^2}\right]_{k_\perp=0}\frac{\partial^2A(y,z,t)}{\partial z^2}=0. \tag{6}$$

The magnetic nonlinearity will now be assumed to add a nonlinear frequency shift of $-[\partial\omega/\partial|A|^2]_{|A|=0}|A|^2$ to Eq. (6). Equation (6), together with the nonlinear term, makes up the *two-dimensional* nonlinear Schrödinger equation

$$i\left[\frac{\partial A}{\partial t}+v_g\frac{\partial A}{\partial y}\right]+\frac{1}{2}\beta_{2\parallel}\frac{\partial^2A}{\partial y^2}+\beta_{2\perp}\frac{\partial^2A}{\partial z^2}-\alpha|A|^2A=0, \tag{7}$$

where the group velocity is $v_g=\partial\omega(k,0)/\partial k$, the *dispersion* coefficient is $\partial^2\omega(k,0)/\partial k^2$, traditionally referred to as $\beta_{2\parallel}$, and the *diffraction* coefficient is $(\partial^2\omega(k,k_\perp)/\partial k_\perp^2)_{k_\perp=0}$, which shall be referred to as $\beta_{2\perp}$. $\alpha=(\partial\omega/\partial|A|^2)_{|A|=0}$ is simply called the nonlinear coefficient. Contact with the Zvezdin and Popkov paper can be made by noting that

$$\frac{\partial\omega}{\partial k_\perp}=\frac{\partial\omega}{\partial k_\perp^2}\frac{\partial k_\perp^2}{\partial k_\perp}=2\frac{\partial\omega}{\partial k_\perp^2}k_\perp, \tag{8a}$$

$$\left(\frac{\partial^2\omega}{\partial k_\perp^2}\right)_{k_\perp=0}=\left[2\frac{\partial}{\partial k_\perp}\left(\frac{\partial\omega}{\partial k_\perp^2}\right)k_\perp+2\frac{\partial\omega}{\partial k_\perp^2}\right]_{k_\perp=0}=2\frac{\partial\omega}{\partial k_\perp^2}. \tag{8b}$$

For solitons to occur, Eq. (7) must be satisfied with coefficients that satisfy the Lighthill criterion.[13,15] In a real experiment, wave damping must, necessarily, occur, and so some quantitative assessment of how important this is must be made. This is usually done computationally by setting the right-hand side of Eq. (7) equal to $-i\omega_r A$. $\omega_r=\gamma\Delta H$ and is called the relaxation frequency, γ is the gyromagnetic ratio,

and $2\Delta H$ is the ferromagnetic resonance linewidth. Although the possibility of damping is acknowledged, the following discussion omits the $i\omega_r A$ term only for clarity of development. Once $-i\omega_r A$ is added to Eq. (7), it is no longer the Schrödinger equation; i.e., it is no longer integrable. The usual treatment is then to observe the solutions computationally to try and determine if damping can be treated as a perturbation. In this way some information can be fed into the interpretation of the experiments. Briefly, damping tends to broaden fundamental solitons and drive them below threshold.

The solution of Eq. (7) may be unstable to longitudinal or transverse modulations, and it is these instabilities that lead, ultimately, to the formation of solitons. For diffraction to be balanced by self-focusing, the following Lighthill criterion must be satisfied:

$$\beta_{2\perp}\alpha<0. \tag{9}$$

Equation (9) is a necessary condition for self-channeling of the magnetostatic wave beam to occur, together with the absence of longitudinal (dispersion) effects. If this condition is strictly enforceable, then, experimentally, evolution of a beam into a spatial soliton can occur. The sign of the diffraction coefficient $\beta_{2\perp}$ is easily obtained from the *linear* magnetostatic wave dispersion relation and is found to be positive for backward volume waves and negative for surface waves. The nonlinear coefficient α is negative for both surface waves and backward volume waves.[14] Therefore the criterion (9) is satisfied for backward volume waves, but not for surface waves, which allows, at least, the possibility of self-channeling in backward volume waves. For solitons to exist, the magnetostatic wave must be unstable to perturbations in one dimension only. If a wave is unstable to perturbations both parallel and transverse to the direction of propagation, then the two-dimensional nonlinear Schrödinger equation applies and unstable solutions ensue. If this happens, then self-channeling may not be seen, nor, indeed, will spatial solitons.

A beam is cw with respect to time and is unstable to longitudinal (parallel) perturbations when

$$\beta_{2\|}\alpha<0. \tag{10}$$

In fact, a cw signal which obeys this condition should, after some propagation distance, exhibit the kind of modulation instability that, over a long period of time, leads to envelope (temporal) solitons. This condition is certainly obeyed for backward volume waves, though it is not for surface waves. When observing backward volume wave beams, therefore, in an attempt to find self-channeling, it is important to operate under conditions where modulation instability due to longitudinal perturbations is negligible. If this can be arranged, then only diffraction and nonlinearity remain, and the amplitude of a backward volume wave beam is a solution of the one-dimensional nonlinear Schrödinger equation[13]

$$iv_g\frac{\partial A}{\partial y}+\beta_{2\perp}\frac{\partial^2 A}{\partial z^2}-\alpha|A|^2A=0. \tag{11}$$

Now only diffraction and self-focusing possibilities are included and stable stationary (soliton) states will exist. If this cannot be arranged, then it must be accepted that nonlinear backward volume self-focused waves are going to be influenced by longitudinal modulational instability. The use of Eq. (11) as a description of the self-channeling of backward volume wave beams is rather limited, therefore. Unfortunately, a comprehensive theory of the two-dimensional nonlinear Schrödinger equation, appropriate for a description of the properties of nonlinear magnetostatic waves, is not available in the literature, and so some comments on the limits on their observation will be presented later on in this section.

Even when the one-dimensional nonlinear Schrödinger equation is an appropriate description, the condition $\beta_{2\perp}$, $\alpha<0$ is not sufficient for the existence of self-channeling. The peak power of the magnetostatic beam must also exceed a certain critical value. This can be appreciated by casting the nonlinear Schrödinger equation into a dimensionless form. The coordinate z can be measured in terms of the beam half-width D_0, and the y coordinate can be measured in units of $L_D=|2v_gD_0^2/\beta_{2\perp}|$, so that (11) becomes

$$i\frac{\partial U}{\partial\xi}+\mathrm{sgn}(\beta_{2\perp})\frac{\partial^2 U}{\partial\eta^2}-\mathrm{sgn}(\alpha)\frac{L_D}{L_{\mathrm{NL}}}|U|^2U=0, \tag{12}$$

where $y=\xi L_D$ and $z=\eta D_0$. L_D is called the *diffraction length*, and here L_D is the distance over which diffraction will cause a typical beam (e.g., Gaussian shape) to double its width in a lossless medium. In this normalization, the *magnetostatic wave amplitude* A is written as $A(y,z)=\sqrt{\Gamma}U(\xi,\eta)=\sqrt{\Theta P_0}$, where Γ is introduced to make U dimensionless. $L_{\mathrm{NL}}=|v_g/\alpha\Theta P_0|$ is called a *nonlinear length*; the parameter Θ is simply a normalization factor, which permits P_0, the peak power, to be expressed in watts. L_{NL} is called a nonlinear length because it is the distance over which the nonlinearity tends to become important. In a material without losses, this length is that over which the maximum nonlinear phase shift in the beam is equal to unity. When a soliton is formed, $(L_D/L_{\mathrm{NL}})^{1/2}$ gives the order of the soliton, which will have an integer value for such a stationary state.

The parameter $\beta_{2\perp}$ is found from the *linear* magnetostatic wave dispersion relation, and hence the diffraction length L_D can easily be calculated. Provided that Eq. (2) is satisfied, Eq. (6) has the lowest-order soliton solution when $L_D/L_{\mathrm{NL}}=1$ and the threshold peak power of this soliton is

$$P_0=\frac{2\beta_{2\perp}}{\Theta\left(\dfrac{\partial\omega}{\partial|A|^2}\right)D_0^2}. \tag{13}$$

In a *lossless* medium, a beam, with an initial sech-type profile, will form into a fundamental soliton if, initially, $0.5<(L_D/L_{\mathrm{NL}})^{1/2}<1.5$. In this case, the threshold power required for formation of a fundamental soliton is a quarter of the peak power implied by the stationary state condition, Eq. (13). This power threshold relationship needs modification for the experiment reported here because the initial beam shape should have more of a square profile. For example, if a true square, or rectangular, input profile could be generated, then a first-order soliton forms when $0.5\pi<(L_D/L_{\mathrm{NL}})^{1/2}<1.5\pi$.[13] Also, in reality, the beam propagates in a medium *with losses*, and so, although the above

TABLE I. Parameters for backward volume waves.

f [GHz]	$k_\parallel$ [cm^{-1}]	Calculated $\lvert v_g\rvert$ [cm s^{-1}]	Measured $\lvert v_g\rvert$ [cm s^{-1}]	L_D [cm]
5.82	56.3	3.61×10^6	3.54×10^6	0.43
5.80	91.3	3.56×10^6	3.50×10^6	0.69
5.75	181.0	3.44×10^6	3.40×10^6	1.34

equations can still be used to make estimates of the power levels involved, care must be taken to make an appropriate allowance for these facts.

Tables I and II display estimated parameters that are appropriate to the experiments on backward volume and surface waves that are reported here, calculated from the relevant dispersion relations and assuming that the initial beam width is equal to the length of the antenna generating the beam. The values of v_g measured from linear pulse delay experiments are also shown. It was not possible experimentally to measure the width and shape of the initial magnetostatic wave beam, using Brillouin light scattering, and this will be discussed later. For backward volume waves, it can be seen that, as the frequency of the wave decreases, the diffraction length L_D increases. This means that the diffraction is weaker, and so *less* power is needed to reach the threshold condition as the frequency is reduced. Solitons typically form over a distance equal to L_D, and the propagation distance of spin waves is restricted by magnetic losses, which means that, at a typical distance from the input antenna, where self-channeling could occur, the intensity of the wave is strongly reduced. The unfortunate consequence of loss is that only the *initial stage* of soliton formation may be seen, before losses reduce the power below the threshold required for soliton formation.

Modulational instability[13,15] is a description of what happens to a cw wave upon entering a nonlinear medium, when the Lighthill criterion is satisfied. If such an instability ensues, it will filament, or break up, the wave. In the present context, it is necessary to determine if beam breakup due to such perturbations can occur. The perturbations are called longitudinal because they are associated with the propagation direction, and the main question is whether they can suppress the formation of backward volume wave spatial solitons. If loss is ignored, for the moment, then the gain of this type of instability, for a wave of dimensionless amplitude U, is[15]

$$\text{gain}=\left|\frac{2\,\dfrac{\partial\omega}{\partial|U|^2}\,|U|^2}{v_g}\right|,$$

where v_g is the group velocity. Hence the amplitude I of the instability, after a distance z, will be given by

TABLE II. Parameters for surface waves.

f [GHz]	$k_\parallel$ [cm^{-1}]	Calculated $\lvert v_g\rvert$ [cm s^{-1}]	Measured $\lvert v_g\rvert$ [cm s^{-1}]	L_D [cm]
5.905	34.9	4.37×10^6	4.7×10^6	0.41
5.970	135.8	3.74×10^6	4.0×10^6	1.36

$$I(z)=I_0\,\exp\left(\frac{2z\left|\dfrac{\partial\omega}{\partial|U|^2}\right||U|^2}{|v_g|}\right).$$

Clearly, such modulation instability will only become important beyond a certain propagation distance. If losses are included, the following condition[3] must be satisfied in order to observe modulational instability:

$$L\gg\frac{|v_g|}{\left|\dfrac{\partial\omega}{\partial|U|^2}\right||U|^2-\omega_r}.$$

Beam profiles are measured up to a distance of 5.5 mm in this experiment, and taking typical parameters calculated for our backward volume wave experiment at 5.82 GHz (see next section for details), $\partial\omega/\partial|U|^2=-7.39\times10^9$ s^{-1} and $|v_g|=3.61\times10^6$ cm s^{-1}. It is clear that modulation instability will be important only if $|U|^2\gg1.72\times10^{-3}$. In a lossless medium, assuming a sech-like initial beam profile, we may expect a soliton to form if, initially, $L_D/L_{\rm NL}$ is roughly 0.25. Assuming an initial beam width of 0.14 cm, a soliton should form when $|U|^2>2.8\times10^{-4}$. Thus, even allowing for the losses in such a YIG film, it is realistic to expect spatial soliton formation without degradation from longitudinal modulation instability. Obviously, there is always a danger of this, at higher powers, and the conditions must be carefully selected and each parameter range carefully assessed.

III. DISCUSSION OF THE EXPERIMENTAL RESULTS

Experimental beam profiles have been measured using a YIG single crystal film possessing a thickness of 7.2 μm. To avoid any nonuniformity of the internal magnetic field, a wide piece of YIG (over 1 cm) was used. The full spin-wave resonance linewidth $2\Delta H$, measured at 5 GHz was 0.7 Oe, and other film parameters were $\gamma=2.8$ MHz/kOe and $4\pi Ms=1750$ G. A gold microstrip transducer 20 μm wide and 1.4 mm long, deposited on alumina, was used to generate the beam, and a second output transducer, 1.14 cm farther away, was used to monitor the signal transmitted between them. An electromagnet provided a constant external magnetic field, in the plane of the YIG film. This external field was strictly parallel to the input transducer when surface waves were generated and was perpendicular to the transducer when generating backward volume waves in order to avoid any energy steering effect.[7] The magnetic field was carefully chosen to avoid the possibility of three-magnon decay processes, which can occur at very low power levels. The experimental set up is shown in Fig. 1.

Light from an argon ion laser of wavelength 514 nm was focused onto the YIG film with an estimated spot size of 25 μm. A proportion of this light will undergo Brillouin scattering from the magnetostatic waves in the film and be shifted in frequency from the incident light by an amount equal to the frequency of the magnetostatic waves. Such light is collected on the other side of the YIG film and is steered to the interferometer using suitable optics. The amount of light which is frequency shifted is proportional to the magnetostatic wave intensity. Therefore, by measuring the Brillouin scattered light intensity, at a sufficiently large

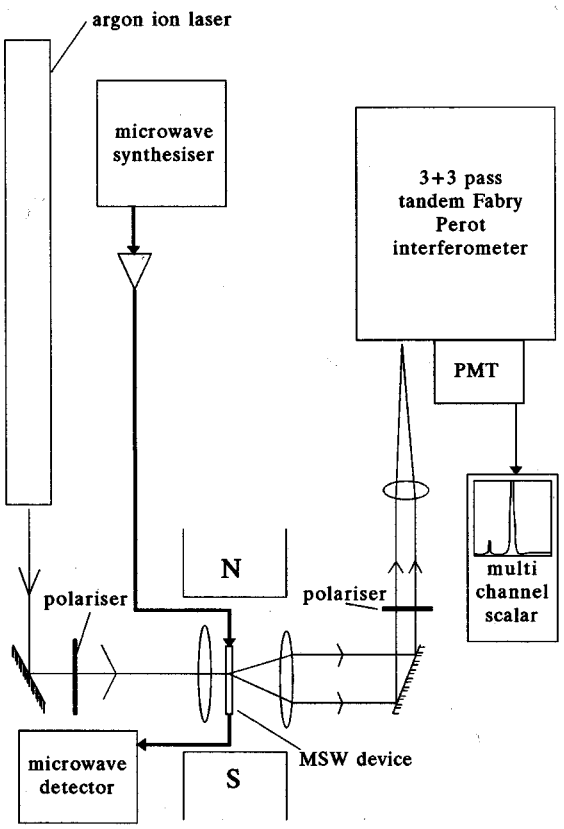

FIG. 1. Details of experimental setup. Linearly polarized light from an argon ion laser is focused onto the magnetostatic wave device consisting of an in-plane magnetized YIG film and stripline antennae. Light passing through the film is analyzed using a multiple-pass Fabry-Pérot interferometer, and the results displayed on a multiple-channel analyzer.

number of points, it is possible to define the shape of the magnetostatic wave beam. In order to measure the cross section profile of a beam, measurements were taken in steps of 250 μm perpendicular to the direction of the beam. The YIG film was mounted on a translation stage whose positions could be accurately measured using micrometer screw gauges.

Figure 2 shows a typical Brillouin light scattering spectra obtained, when light has been scattered from the backward volume wave at a frequency of 5.82 GHz with input power of 100 mW. Two peaks are visible, a large central peak (1) of Rayleigh scattered light at the frequency of the incident radiation, and a much smaller peak on the right (2) caused by Brillouin light scattering from magnetostatic waves. On the vertical scale selected here, only the base of peak (1) is seen. The height of the peak due to Brillouin scattering is proportional to the magnetostatic wave intensity at the position on the YIG film where the light is focused. By measuring the height of this peak at several positions, the beam cross section, shown in Fig. 3, was measured. This cross section is measured at a propagation distance of $y=1.5$ mm. The horizontal scale gives the position (z) on the YIG film, in mm, simply measured from a point close to the film edge. The vertical scale is the number of photons counted, proportional to the magnetostatic wave intensity at the point (y,z). The graduation marks on the horizontal scale show each position

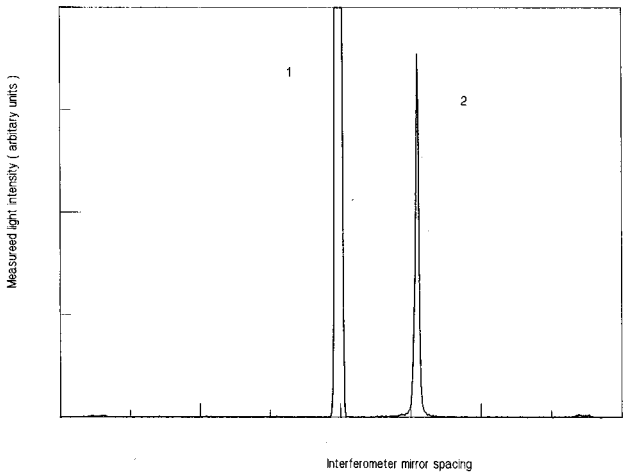

FIG. 2. Brillouin light scattering data obtained from backward volume waves at 5.82 GHz. The measured light intensity is plotted against the interferometer mirror spacing. Peak (2) is that of photons shifted in frequency from the center peak (1), which is at the frequency of the incident light. The height of peak (2) is proportional to the magnetostatic wave power. Since the actual value of mirror spacing is unimportant, it is shown in arbitrary units.

at which the magnetostatic wave intensity was measured. The intensity of the magnetostatic wave in this figure is given in arbitrary units. This is, in fact, the number of photons detected over a specific time length for a constant laser power. Since the aim was to measure the shape of the magnetostatic wave beam, relating this photon count to the actual magnetostatic wave intensity, which would require a comprehensive theoretical effort, is unnecessary at this stage. In order to allow comparison of relative beam intensities, in all figures, the conditions under which Brillouin light scattering intensities were measured, for each data point, were always

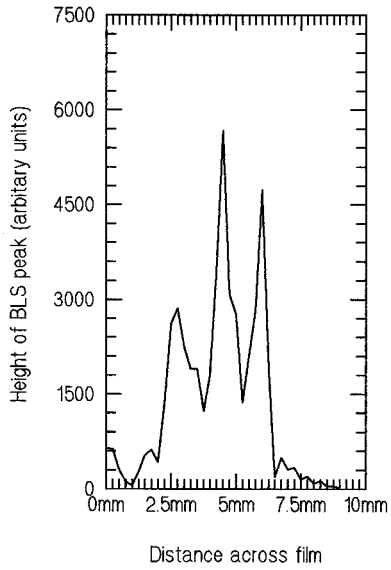

FIG. 3. Shape of a backward volume wave beam recorded 1.5 mm from the input antenna: the frequency is 5.82 GHz and input power is of 100 mW. The horizontal scale shows the position on the film, and the vertical scale shows the measured scattered intensity, which is proportional to the magnetostatic wave intensity.

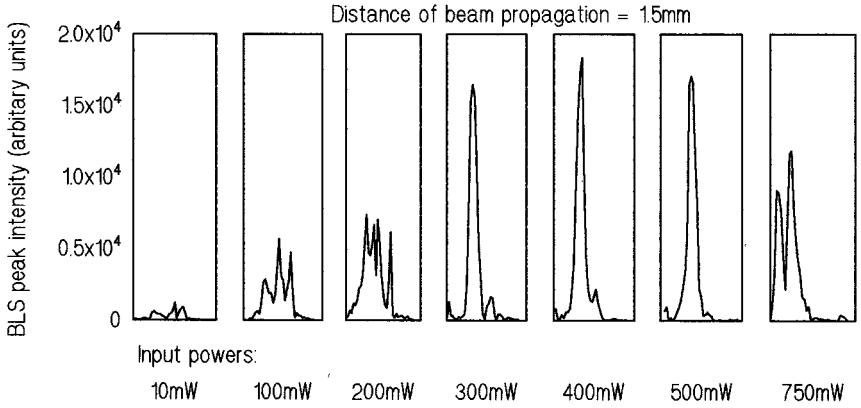

FIG. 4. Beam profiles obtained from Brillouin light scattering measurements, showing the change of backward volume wave beam shape with power, 1.5 mm from the input antenna at a frequency of 5.82 GHz and with an internal magnetic field of 1391 Oe. Each cross section is measured over a distance of 11 mm, at steps of 250 μm. Scattered intensity (i.e., the number of photons, which is proportional to magnetostatic wave intensity) is plotted on the vertical axis. The beam profiles correspond to input powers of 10, 100, 200, 300, 400, 500, and 750 mW, with power increasing from left to right.

identical. The beam shape in Fig. 3 is rather curious, having a peaked structure, and at this distance is fairly wide in comparison to the size of the 1.4-mm antenna used in its generation. It is observed, however, that the intensity is concentrated at the film center, and therefore it should be possible to demonstrate the influence of power on the beam shape.

A series of such measurements for backward volume waves under the same conditions as those used to generate Fig. 3 is shown in Fig. 4 for various power levels and at $y=1.5$ mm from the input antenna. The internal magnetic field was estimated to be 1391 Oe. The diffraction length calculated for these beams is 0.43 cm, which is relatively short. At low input powers, i.e., 10–100 mW, the beam is quite broad, considering that such a short 1.4-mm transducer was used, and multiple peaks can be seen. At 200 mW the beam has narrowed slightly. For powers of 300–500 mW, a narrow channel has been formed. It is also interesting to notice that, for these powers, the peak intensity has saturated and that, finally, at 750 mW, the beam has broadened and split.

In Fig. 5 it can be seen how these beams evolve, because beam profiles for propagation distances equal to 3.5 and 5.5 mm are also shown. The beam profiles are arranged into rows which contain results for the *same propagation distance* and columns that contain results at the *same input power*. The propagation distance increases from the top to

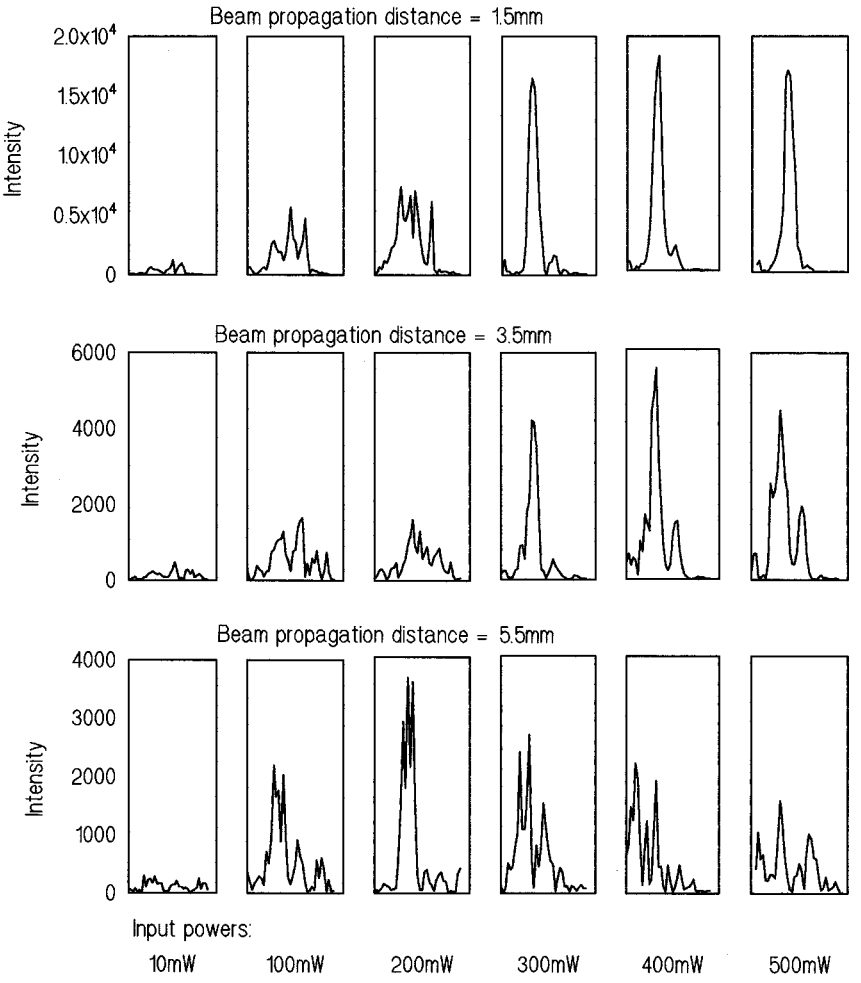

FIG. 5. Evolution of backward volume wave beams with frequency 5.82 GHz taken at three distances from the input antenna. Each cross section is measured over 11 mm. Input beam power levels are 10, 100, 200, 300, 400, and 500 mW and increase from left to right. Distances from input antenna are 1.5, 3.5, and 5.5 mm. The internal magnetic field is 1391 Oe.

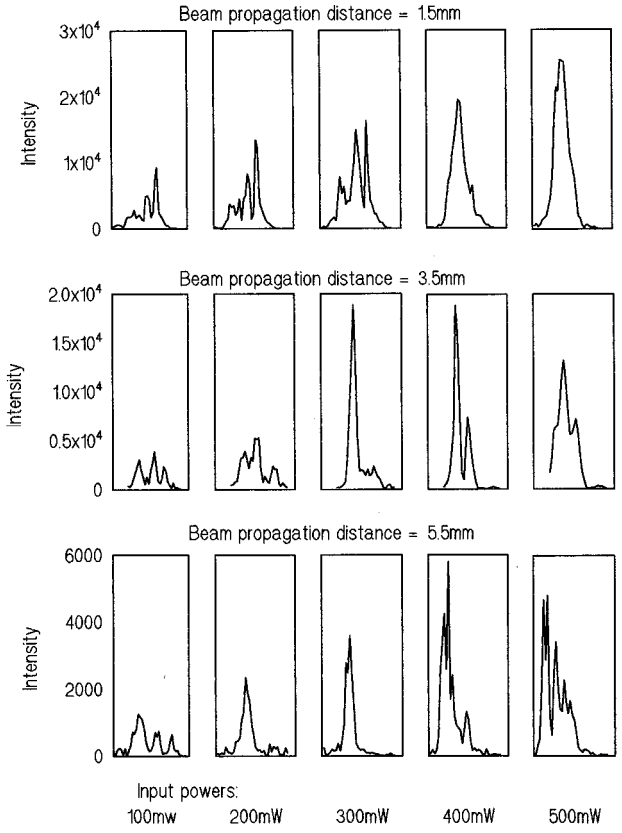

FIG. 6. Evolution of backward volume wave beam with a frequency of 5.80 GHz. Input beam power levels are 100, 200, 300, 400, and 500 mW. Beam profiles at propagation distances of 1.5, 3.5, and 5.5 mm are shown. Internal magnetic field is 1391 Oe.

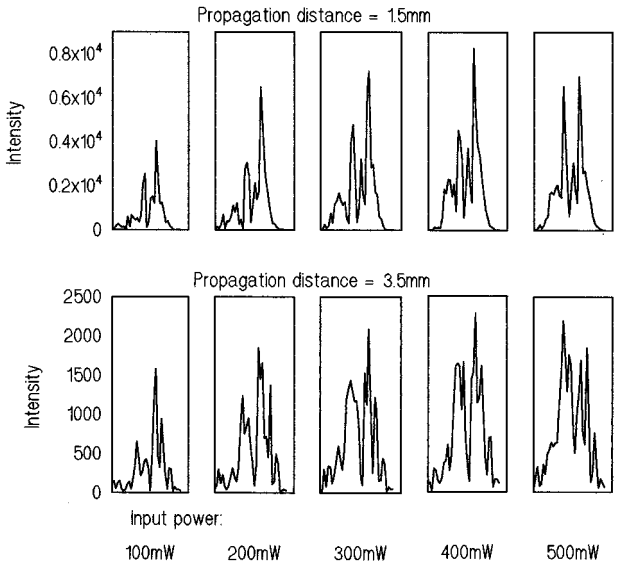

FIG. 7. Evolution of backward volume wave beams with a frequency 5.75 GHz taken at propagation distances of 1.5 and 3.5 mm. Input beam power levels are 100, 200, 300, 400, and 500 mW. Internal magnetic field is 1391 Oe.

the bottom, and the power increases from left to right. It should be emphasized that the powers quoted are the powers coupled from the antennae, i.e., the difference in the power delivered to the antenna and the power reflected from it. It is very difficult to estimate, accurately, how much of this power actually couples into the magnetostatic wave beam, especially in the nonlinear regime, but it will be lower than these input powers. In Fig. 5, for input powers of 10 and 100 mW, it is seen that the intensity of beams weakens during propagation and no self-channeling can be seen. In fact, the beams are broad and multipeaked. As the initial power is increased, sharp, narrow, beams are formed, with a stable propagation width. A point worth making here is that, for a power of 200 mW, narrowing and formation a self-channeled beam were visible only at a distance of 5.5 mm. Another feature which is easily visible in Fig. 5 is that the peak of the maximum intensity is slightly shifted to the left-hand side. This can be attributed to a small amount of beam steering,[7] possibly due to the fact that the external magnetic field was not exactly perpendicular to the input antenna.

The next set of results is shown in Fig. 6 and was obtained under the same conditions, but at a frequency of 5.80 GHz. Here the diffraction length is calculated to be 0.69 cm, which is longer than for the data given in Fig. 5, and so the evolution length for self-channeling is expected to be longer. The experimental evidence seems to confirm this, since, with a power level of 300 mW, a narrow channel did not form until the beam had propagated 3.5 mm and it was still visible at 5.5 mm. In Fig. 6, at input power levels of 300 and 400 mW, the beam width narrows to as low a value as 2 mm, after propagation 3.5 mm.

The last set of results for backward volume waves is shown in Fig. 7. These results were obtained for propagation distances of 1.5 and 3.5 mm, under similar conditions as in the previous cases, but at a frequency of 5.75 GHz. Some small change in beam profile is seen when power is increased, but there is no self-channeling. Since the calculated diffraction length is 1.34 cm, it is likely that the distance over which the beam can propagate with high power is shorter than that required for soliton formation.

Two frequencies were used to investigate surface waves, and Fig. 8 shows that self-defocusing of surface waves was observed at propagation distances of 1.5 mm for a frequency of 5.905 GHz and internal field of 1400 Oe. As the observation distance increased, most of the beam energy was steered from the linear direction of propagation at high input powers. This surface wave beam behavior, when the energy is steered away from the center of the beam, can be found for linear waves[11] and is caused by the anisotropic properties of surface waves. Analysis of dispersion and group velocity of surface waves[10] gives the directions of dominant energy transport, which, in the linear regime, do not always coincide with the expected direction of propagation of the beam. Increasing the power of surface waves actually assists defocusing so that, at higher powers, beams become even wider and have much more irregular shape. When the frequency was increased to 5.97 GHz, thereby increasing the diffraction length, a similar evolution was seen, shown in Fig. 9.

The calculated nonlinear lengths L_{NL} for backward volume and surface waves are presented in Table III, assuming that all the power input via the antenna coupled into magnetostatic waves. These values suggest that the condition $L_{\mathrm{NL}}=L_D$ is easily fulfilled for backward volume waves when the initial power is 100 mW. In most cases the nonlinear

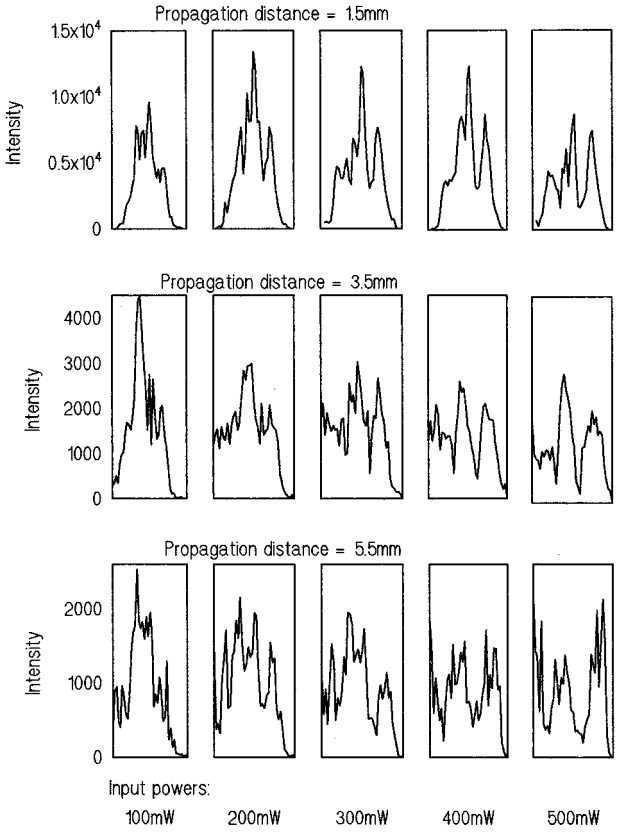

FIG. 8. Evolution of surface wave beams when the internal field is 1400 Oe, and at a frequency of 5.905 GHz. Propagation distances are 1.5, 3.5, and 5.5 mm. Beam input power levels are 100, 200, 300, 400, and 500 mW.

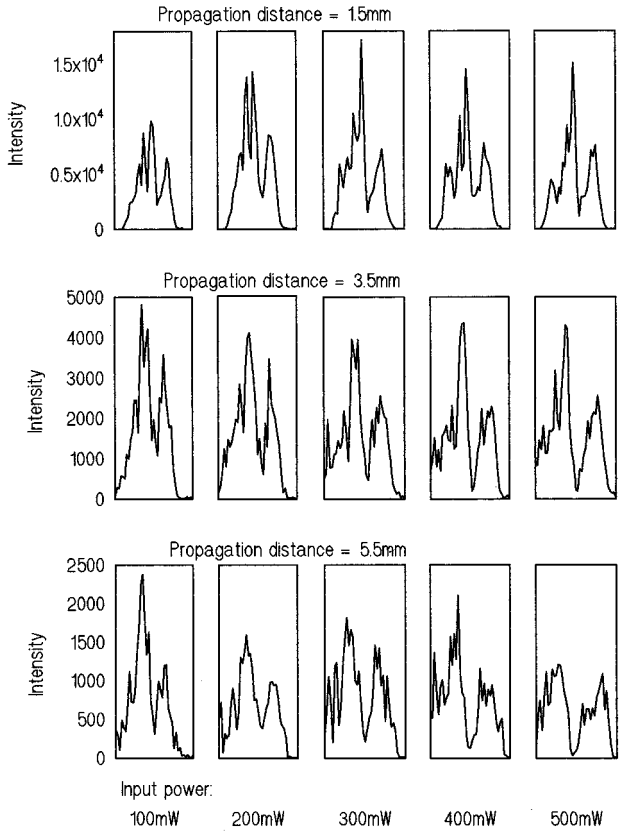

FIG. 9. Evolution of surface wave beams at a frequency 5.97 GHz. Other parameters are as for Fig. 8.

length L_{NL} is smaller, or much smaller, than the diffraction length L_D. These values may only be a rough guide to the actual properties of the magnetostatic wave beam found in these experiments. To accurately calculate L_D requires additional knowledge such as the width and shape of the initial beam generated by the antenna. Unfortunately, since the antenna requires the presence of a metal ground plane, which blocks the laser light in its vicinity, we can only perform Brillouin light scattering experiments after the beam has propagated a short distance. Also, near the antenna, other non-propagating spin waves, which might also be generated, may be detected, giving a misleading idea of the initial beam shape. It is likely that the beam width is similar to the length of the antenna and that these values of L_D are fairly accurate. In estimating the value of L_{NL} it is necessary to know the power in the beam. Since not all the power in the antenna will couple into the magnetostatic wave, actual values of L_{NL} are likely to be longer. Despite such possible uncertainties in these values, they should give a feel for the experimental conditions in which spatial solitons can form.

Clearly, the results reported here show evidence of self-channeling of backward volume waves, as the input power is increased, and an increase in diffraction with increasing input power for surface waves, because of self-defocusing. However, it is not altogether clear whether this self-channeling is in fact a spatial soliton or merely the initial stages of spatial soliton formation, since the conditions which must be fulfilled before something can accurately be claimed to be a soliton are rather strict. After some distance, for high powers the channeled region is lost and the beam resumes the multiple-peaked structure found at low power. This could be due to losses reducing the beam power below the threshold for soliton formation or possibly due to the onset of modulational instability, making a soliton unstable. It is interesting to note that the peak height does not increase linearly with input power in these beams, suggesting some nonlinear loss mechanism, possibly due to heating of the sample by the magnetostatic wave power or a coupling of power into spin-wave modes. It should be noted that at lower powers, e.g., below 10 mW, not only did the measured beam intensity increase linearly with input power, but the same multiple-peaked structure was reproducible at different powers.

Possible limitations on the use of the nonlinear Schrödinger equation to describe these beams should be noted.

TABLE III. Estimated value of nonlinear length.

Input power [mW]	L_{NL} [cm] volume waves	L_{NL} [cm] surface waves
10	1.244	2.146
100	0.124	0.219
200	0.062	0.107
300	0.042	0.072
400	0.032	0.054
500	0.024	0.043

First, the nonlinear Schrödinger equation is derived from a Taylor expansion, ignoring higher-order terms, and it is generally assumed that the wave number spread Δk satisfies $\Delta k \ll k$, where k is the carrier wave number. For low-power backward volume wave beams, at 5.82 GHz, the angle of beam divergence, by careful examination of the results from 1.5 to 5.5 mm, is seen to be roughly 25°. This raises the question of whether this condition is truly satisfied. Two things must be remembered, however. First, as mentioned earlier, due to the anisotropic nature of the dispersion branches for these waves, the directions of energy flow are generally not parallel to the direction of the wave vector.[7,8] In fact, in the cases considered here, for a backward volume wave beam parallel to the applied magnetic field and for a surface wave beam perpendicular to it, then for a wave vector, orientated at some angle to the direction of propagation of the beam, the direction of energy flow associated with that wave vector will be at some larger angle with respect to the beam direction. Therefore the value of Δk will be smaller than indicated by observing the divergence of energy in the beam. Second, even when this condition is not obeyed, such a Taylor expansion will not automatically become invalid, if higher-order terms can still be ignored. The nonlinear Schrödinger equation can be used for large Δk depending on the shape of the dispersion curve in question. To use the nonlinear Schrödinger equation, it is necessary to ensure that the dispersion relation can be represented by a Taylor expansion which converges rapidly. The dispersion curves for the magnetostatic waves considered here are smooth, and the derivatives in the Taylor expansion vary slowly along it. The higher-order terms are also small. Therefore it is believed, for these experiments, that the use of the nonlinear Schrödinger equation is valid for the beams investigated. However, *exact modeling* using the nonlinear Schrödinger equation will be difficult without knowing the initial change in phase across the beam, that is probably generated using these short striplines. It is also realistic to expect, at high powers, that the antenna will generate beams with some kind of chirp, i.e., with curved wave fronts, as a result of the intensity distribution across the initially generated beam width, further complicating analysis of such data.

In conclusion, measurements of self-channeling and nonlinear beam formation of *backward volume* magnetostatic waves have been reported. We also present the experimental confirmation that magnetostatic *surface* waves do not give rise to self-channeling. Indeed, at low wave numbers they quickly defocus as they propagate. All features of nonlinear beam shaping can be discussed qualitatively in terms of the nonlinear Schrödinger equation.

ACKNOWLEDGMENTS

We gratefully acknowledge J. D. Adam of the Westinghouse Research and Development Centre, Pittsburgh, PA for providing the YIG films; Anritsu Wiltron, Kansas Avenue, Langworthy Park, Salford, UK, for the loan of a synthesized signal generator, and the UK Defence Research Agency, Maritime Division (Funtington) for support. One of us (S.A.N.) is indebted to the Alexander von Humboldt Foundation for financial support during this work.

*On leave from the Radioengineering and Electronics Institute, Russian Academy of Sciences, 103 907, Mokhovaya St, 11 Moscow, Russia.

[1] B. A. Kalinikos, N. G. Kovshikov, and A. N. Slavin, JETP Lett. **38**, 413 (1983).

[2] P. De Gasperis, R. Marcelli, and G. Miccoli, Phys. Rev. Lett. **59**, 481 (1987).

[3] B. A. Kalinikos, N. G. Kovshikov, and A. N. Slavin, Sov. Phys. JETP **67**, 303 (1988).

[4] M. Chen, M. A. Tsankov, J. M. Nash, and C. E. Patton, Phys. Rev. B **49**, 12 773 (1994).

[5] M. A. Tsankov, M. Chen, and C. E. Patton, J. Appl. Phys. **76**, 4274 (1994).

[6] M. Chen, M. A. Tsankov, J. Nash, and C. E. Patton, Phys. Rev. Lett. **70**, 1707 (1993).

[7] F. A. Pizzarello, J. H. Collins, and L. E. Coerver, J. Appl. Phys. **41**, 1016 (1970).

[8] S. N. Bajpai, J. Appl. Phys. **50**, 6564 (1979).

[9] N. P. Vlannes, J. Appl. Phys. **61**, 416 (1987).

[10] A. V. Vashkovskii, A. V. Stal'makhov, and D. G. Shakhnazaryan, Sov. Phys. J. **31**, 908 (1988).

[11] N. P. Vlannes, J. Appl. Phys. **62**, 972 (1987).

[12] K. V. Greschuskin, A. V. Stal'makhov, and V. A. Tyulyukin, Sov. J. Commun. Technol. Electron. **37**, 13 (1992).

[13] A. K. Zvezdin and A. F. Popkov, Sov. Phys. JETP **57**, 350 (1983).

[14] The sign of α, for magnetostatic surface waves, is incorrect in Ref. 13.

[15] G. P. Agrawal, *Nonlinear Fibre Optics* (Academic, London, 1989).